Chinese J. of Chem. Eng., 5(1) 1－10 (1997)

HYDRODYNAMIC STUDIES ON LOOP REACTORS (Ⅰ) LIQUID JET LOOP REACTORS*

Lin Wencai (林文才)**, **Mao Zaisha**(毛在砂)***
and Chen Jiayong(陈家镛)

Institute of Chemical Metallurgy, Academia Sinica, Beijing 100080, China

Abstract Understanding of hydrodynamics in liquid jet loop reactors is a prerequisite step for the further study of multi-phase flow in loop reactors. A hydrodynamic simulation for liquid jet loop reactors is developed from the first principles of transport phenomena in this paper. The turbulence is taken into account by using the standard k-ε model. This approach is used to study the influence of configuration and viscosity on the hydrodynamics. The results are in very reasonable coincidence to experimental data in literature.

Keywords hydrodynamics, loop reactor, fluid dynamics, numerical simulation

1 INTRODUCTION

Although in chemical engineering and biotechnology loop reactors are especially suitable for heterogeneous gas-liquid, liquid-solid or gas-liquid-solid systems, studies on homogeneous liquid flow in a jet loop system remain important. First, all basic features and general fluid dynamic behaviors of heterogeneous loop reactors can be demonstrated in a simple way by using corresponding homogeneous liquid systems, at least in a qualitative context. Studies on homogeneous systems can serve as a good foundation for developing multi-phase loop reactors[1,2]. Secondly, liquid jet loop reactors are also used for anaerobic fermentation[3] and other purposes such as mixing[4] and liquid lift[5]. To date, liquid jet loop reactor has attracted considerable attention from researchers[1,2,5,6,7]. The objective of this paper is to study the fundamental hydrodynamic features of this type of reactor: a hydrodynamic simulation is conducted, then this approach is used to evaluate the influence of configurational parameters and physical properties on the hydrodynamic behaviors.

2 MATHEMATICAL FORMULATION

2.1 Governing equations

The flow in the unit is considered to be steady, so the continuity and momentum equations are[8]

$$\nabla \cdot U = 0 \tag{1}$$

$$\rho U \cdot \nabla U = -\nabla p + \mu \nabla^2 U \tag{2}$$

Received 1995－12－11, accepted 1996－09－14.

* Supported by the National Natural Science Foundation of China.

** Present address: Research Institute of Petroleum Processing, Beijing 100083.

*** To whom correspondence should be addressed.

When turbulent flow is encountered, viscosity μ is replaced by effective viscosity μ_e. In an axial symmetric cylindrical coordinate system, the governing equations now give

$$\frac{\partial}{\partial x_2}(\rho U_2)+\frac{1}{x_1}\frac{\partial}{\partial x_1}(x_1\rho U_1)=0 \tag{3}$$

$$\frac{\partial}{\partial x_2}(\rho U_2U_1)+\frac{1}{x_1}\frac{\partial}{\partial x_1}(x_1\rho U_1U_1)=-\frac{\partial p}{\partial x_1}+\frac{\partial}{\partial x_2}(\mu_e\frac{\partial U_1}{\partial x_2})+\frac{1}{x_1}\frac{\partial}{\partial x_1}(x_1\mu_e\frac{\partial U_1}{\partial x_1})+S_{U_1} \tag{4}$$

$$\frac{\partial}{\partial x_2}(\rho U_2U_2)+\frac{1}{x_1}\frac{\partial}{\partial x_1}(x_1\rho U_1U_2)=-\frac{\partial p}{\partial x_2}+\frac{\partial}{\partial x_2}(\mu_e\frac{\partial U_2}{\partial x_2})+\frac{1}{x_1}\frac{\partial}{\partial x_1}(x_1\mu_e\frac{\partial U_2}{\partial x_1})+S_{U_2} \tag{5}$$

where

$$\mu_e=\mu+\mu_t \tag{6}$$

and additional source terms S_{U_1} and S_{U_2} are resulted from turbulent inhomogeneity

$$S_{U_1}=\frac{\partial}{\partial x_2}(\mu_t\frac{\partial U_2}{\partial x_1})+\frac{1}{x_1}\frac{\partial}{\partial x_1}(x_1\mu_t\frac{\partial U_1}{\partial x_1})-(\mu_t+\mu_e)\frac{U_1}{x_1^2}$$

$$S_{U_2}=\frac{\partial}{\partial x_2}(\mu_t\frac{\partial U_2}{\partial x_2})+\frac{1}{x_1}\frac{\partial}{\partial x_1}(x_1\mu_t\frac{\partial U_1}{\partial x_2})$$

2.2 Turbulence model

For turbulent flow, the k-ε model[9] has been proven to be suitable for many cases of practical importance. In this model, turbulent viscosity μ_t is related to two transportable properties, the turbulent kinetic energy k and the energy dissipation ε

$$\mu_t=C_\mu\rho\frac{k^2}{\varepsilon} \tag{6}$$

where C_μ is an empirical constant. The k and ε in equations are respectively

$$\frac{1}{x_1}\frac{\partial}{\partial x_1}(x_1\rho U_1k)+\frac{\partial}{\partial x_2}(\rho U_2k)=\frac{1}{x_1}\frac{\partial}{\partial x_1}[x_1(\mu+\frac{\mu_t}{\sigma_k})\frac{\partial k}{\partial x_1}]+\frac{\partial}{\partial x_2}[(\mu+\frac{\mu_t}{\sigma_k})\frac{\partial k}{\partial x_2}]+p-\varepsilon \tag{7}$$

$$\frac{1}{x_1}\frac{\partial}{\partial x_1}(x_1\rho U_1\varepsilon)+\frac{\partial}{\partial x_2}(\rho U_2\varepsilon)=\frac{1}{x_1}\frac{\partial}{\partial x_1}[x_1(\mu+\frac{\mu_t}{\sigma_\varepsilon})\frac{\partial \varepsilon}{\partial x_1}]+\frac{\partial}{\partial x_2}[(\mu+\frac{\mu_t}{\sigma_\varepsilon})\frac{\partial \varepsilon}{\partial x_2}]+C_1\frac{\varepsilon}{k}p-C_2p\frac{\varepsilon^2}{k} \tag{8}$$

where p is the source of turbulent energy

$$p=\mu_t[(\frac{\partial U_2}{\partial x_1}+\frac{\partial U_1}{\partial x_2})^2+2(\frac{\partial U_2}{\partial x_2})^2+2(\frac{\partial U_1}{\partial x_1})^2]+2\mu_e(\frac{U_1}{x_1})^2$$

The standard model constants C_μ, C_1, C_2, σ_k and σ_ε are taken from Jones and Launder[9]

C_μ	C_1	C_2	σ_k	σ_ε
0.09	1.44	1.92	1.0	1.3

3 NUMERICAL IMPLEMENTATION

The numerical implementation is described briefly here; details of numerical procedures can be found in literature[6, 10].

3.1 Discretization scheme

The above transport equations can be written in a general form such as

$$\frac{\partial}{\partial x_2}(\rho U_2\Phi)+\frac{1}{x_1}\frac{\partial}{\partial x_1}(x_1\rho U_1\Phi)-\frac{\partial}{\partial x_2}(\Gamma_{x_2}\frac{\partial\Phi}{\partial x_2})-\frac{1}{x_1}\frac{\partial}{\partial x_1}(x_1\Gamma_{x_1}\frac{\partial\Phi}{\partial x_1})=S_\Phi \qquad (9)$$

To solve the above elliptic partial differential equation, an efficient numerical algorithm of numerical stability and accuracy is required. The Power-Law Scheme (PLS) is adopted for this purpose[10]. Eq. (9) is discretized on a staggered grid system by the control volume method[6, 10]. All scalar quantities are designated on the same grid points, and nodes for velocity components are displaced on the cell faces between two adjacent nodes. The finite-volume control regions for U_1, U_2 and p are shown in Fig.1. Thus, Eq.(9) is discretized on these cells to a set of algebraic equations

$$a_P\Phi_P=a_E\Phi_E+a_W\Phi_W+a_N\Phi_N+a_S\Phi_S+b \qquad (10)$$

where

$$a_E=D_eA(|p_e|)+[\![-F_e,\ 0]\!]$$

$$a_W=D_wA(|p_w|)+[\![F_w,\ 0]\!]$$

$$a_N=D_nA(|p_n|)+[\![-F_n,\ 0]\!]$$

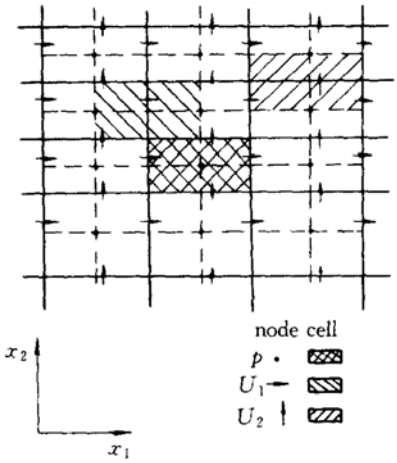

Figure 1 A staggered distribution of nodes in the domain

$$a_S = D_s A(|p_s|) + [\![F_s,\ 0]\!]$$

$$b = S_c \Delta V$$

$$a_P = a_E + a_W + a_N + a_S - S_p \Delta V$$

$$A(|p|) = [\![0,\ (1-0.1|p|)^5]\!]$$

and the symbol $[\![\ ,\ ]\!]$ stands for choosing the item with larger algebraic values.

3.2 Equation solution algorithm

Because of nonlinearity of the governing equations, the equation set must be solved iteratively. In this work, the SIMPLER[10] algorithm is used. Each set of linear equations, which is formulated over its correspondent control regions is solved in an inner iteration. Considering the anisotropic coefficients of algebraic equations due to the high height to diameter ratio, a two-dimensional correction (2DC) coupled with alternating direction implicit (ADI) iteration method[11] is used.

3.3 Boundary conditions

The numerical domain is shown in Fig. 2. The draft tube is treated as a blocked-off region, and the relevant variables are set to be zero therein[10]. The wall-function method is used to the near-wall nodes[9]. Other boundary conditions are the following:

At inlet

$$U_1 = 0$$

$$U_2(r) = U_{MAX}(1 - \frac{r}{R})^{\frac{1}{7}}$$

$$k = (0.035 U_{LM})^2 [2 + 8(\frac{r}{R})^2]$$

$$\varepsilon = k^{1.5}/l_\varepsilon$$

At outlet

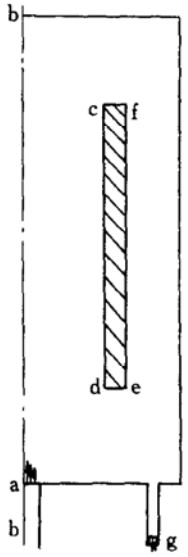

Figure 2 Sketch of the coordinate system and solution domain for a JLR

$$U_1 = 0$$

$$\frac{\partial \Phi}{\partial x_2} = 0$$

On the center line

$$U_1 = 0$$

$$\frac{\partial \Phi}{\partial x_1} = 0$$

3.4 Convergence criteria and effects of grid sizes

Computation is carried out on a PC486 computer. The iterative process is terminated when the relative residuals of the equations less than 10^{-3}. To study the effects of overall grid size on the flow variables, the grid sizes chosen are 38×56, 51×76 and 60×90. It is noted from their contour maps of velocity vectors shown in Fig. 3 that the flow fields in the later two cases are essentially the same. But in the case of a coarse grid, not all recirculations are reflected in the field. So in the subsequent simulation, the medium grid number (51×76) is chosen.

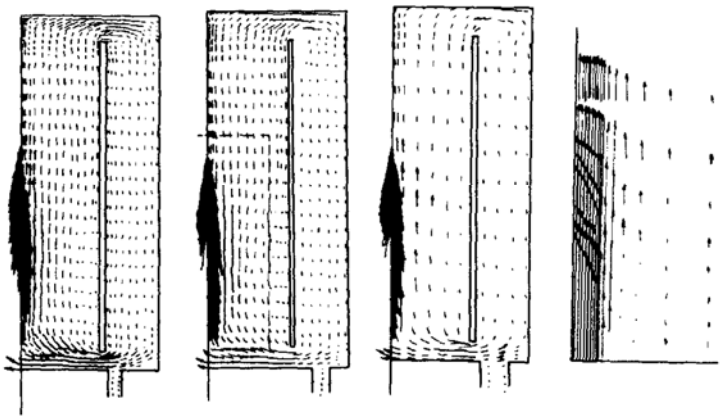

(a) 60×90grid (b) 51×76grid (c) 38×56grid (d) magnification of the dashed line region in (b)

Figure 3 Vector map of velocity for JLR

($s = 5$, $W_1 = 10\text{m} \cdot \text{s}^{-1}$)

4 RESULTS AND DISCUSSION

The numerical program developed is used for a systematic investigation of hydrodynamics in the liquid jet loop reactor. The configurational parameters (see Fig.4) are selected in such a way that the results of simulation may be easily compared with experimental data in the literature[1].

Internal diameter: $D = 0.19\text{m}$

Distance of draft tube from bottom: $A_u = 45\text{mm}$

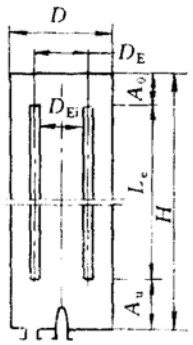

Figure 4 Schematic drawing of a JLR

Distance of draft tube from liquid surface: $A_0 = 65$mm

Height to diameter ratio s: $\frac{H}{D} = 5,\ 10$

Wall thickness of internal tube 0.005m

Diameter ratio: $\frac{D_E}{D} = 0.6$

Liquid viscosity: 0.001 Pa·s

4.1 Analyses on flow fields and comparison with literature data

Typical maps of velocity vectors can be seen in Fig. 3. When the liquid jets into the riser from the nozzle, the mixing of jet stream and circulating liquid from the downcomer takes place at the lower section of the riser. Because the jet velocity is much higher than that of the circulating liquid, the pressure rise caused by mixing of the two streams is greater than the pressure drop of wall friction and adverse pressure gradient is being developed. And a region of recirculation is formed near the jet stream. At the top of the downcomer, another recirculation is formed due to abrupt changes in flow direction. Figs. 5 and 6 present the axial velocity distribution in the radial direction. The flow structure coincides with the literature[7, 12] very well. Blenke[1, 2] conducted a lot of experimental work on the mentioned configuration and defined the following flow

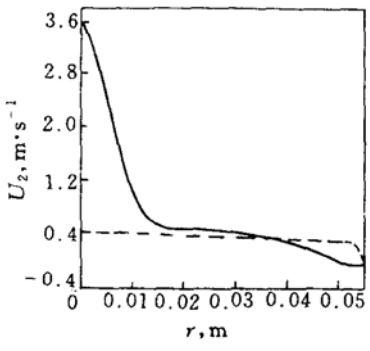

Figure 5 Axial velocity distribution in the riser
($W_1 = 10$m·s^{-1}, $s = 5$)
axial height, m: —— 0.15; ----- 0.82

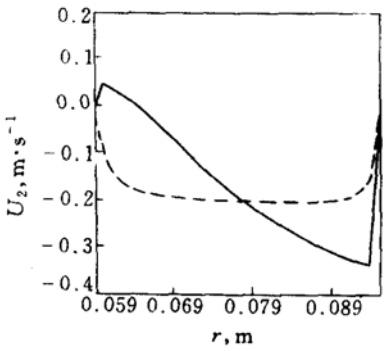

Figure 6 Axial velocity distribution in the downcomer
($W_1 = 10$m·s^{-1}, $s = 5$)
axial height, m: —— 0.96; ---- 0.4

parameters:

1. Mean circulation velocity

$$W_m = 2\ (\dot{M}_1 + \dot{M}_2)\ /(\frac{\pi}{4} D^2 \rho)$$

2. Circulation number

$$n_u = \dot{M}_3/\dot{M}_1 = (\dot{M}_1 + \dot{M}_2)\ /\ \dot{M}_1$$

3. Jet Reynolds number

$$Re_1 = W_1 D_1/v$$

4. Circulation Reynolds number

$$Re_m = W_m D/v$$

Blenke[1, 2] concluded that in the turbulent region

$$\frac{Re_m}{Re_1} = \frac{1}{\frac{250}{Re_1^{1.1}} + 0.84} \tag{11}$$

held valid for $s = 5$, and

$$\frac{Re_m}{Re_1} = \frac{1}{\frac{600}{Re_1^{1.2}} + 0.95} \tag{12}$$

for $s = 10$. Fig. 7 gives the comparison between empirical correlation and numerical prediction. It is found that the results fit quite well.

All the above results suggest that the numerical simulation can be used to predict flow structure and integral flow parameters in close agreement with experimental data. The present numerical approach seems to be reliable and useful in theoretical analysis and numerical experimentation.

4.2 Influence of configurational parameters and viscosity

4.2.1 *Influence of* D/D_E

Numerical and experimental results concerning the effect of diameter ratio on Re_m/Re_1 are shown in Fig. 8. A maximum Re_m/Re_1 exists when D_E/D is around 0.6. This result can be explained from the flow field in Fig.9. When D_E/D is smaller than or equal to 0.36, the recirculation formed at the top section of the downcomer becomes larger as compared with that in Fig. 3 and occupies almost the complete section of the downcomer.

As D_E/D is above 0.8, a large recirculation appears in the riser. Thus, liquid circulating velocity is decreased by the resistance of strong recirculation.

4.2.2 *Influence of* L_e *and* A_u

The influence of the draft tube length L_e on flow can be seen from Fig. 10. When $L_e = 0.306$m, there is a big recirculation atop the riser. Also a dead zone exists in the upper part of the unit. Numerically predicted Re_m/Re_1 in this case is only 0.7. When the spacing between the draft tube A_u is small, Re_m/Re_1 increases with increasing A_u.

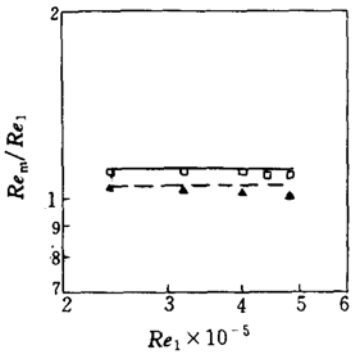

Figure 7 Ratio of Re_m to Re_1 *vs.* Re_1 predicted by this work

□ $s=5$; ▲ $s=10$; —— Eq.(11); ---- Eq.(12)

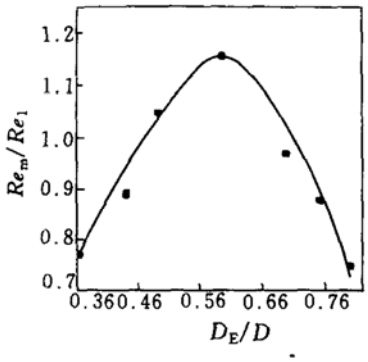

Figure 8 Ratio of Re_m to Re_1 *vs.* D_E/D for $s=5$

—— predicted by this work; ■ expt. of Blenke[1]

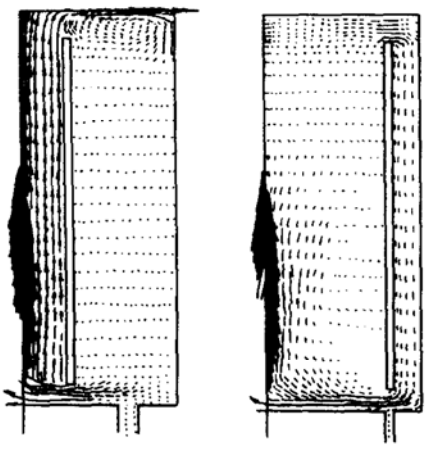

(a) $D_E/D=0.36$ (b) $D_E/D=0.8$

Figure 9 Vector map of velocity for JLR at different diameter ratio ($s=5$, $W_1=10\text{m}\cdot\text{s}^{-1}$)

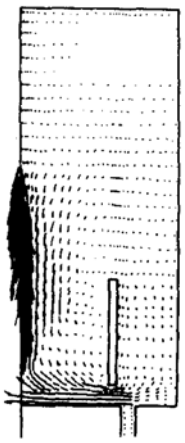

Figure 10 Vector map of velocity vectors for JLR ($s=5$, $W_1=10\text{m}\cdot\text{s}^{-1}$, $L_c=0.306\text{m}$)

Afterwards, the changing Re_m/Re_1 tends to leveled off with increasing A_u (see Fig. 11). This indicates that resistance of the bottom spacing to liquid circulation is no longer the controlling parameter.

4.2.3 *Influence of height to diameter ratio and liquid viscosity*

The influence of height to diameter ratio on Re_m/Re_1 is already presented in Fig.7. Re_m/Re_1 is greater when $s=5$ as compared to that with $s=10$. Numerical results indicate that there is no difference of flow field between $s=10$ and $s=5$. The influence of viscosity on Re_m/Re_1 is shown in Fig. 12. When viscosity is increased, Re_m/Re_1 decreases because of the increased flow resistance due to liquid viscosity.

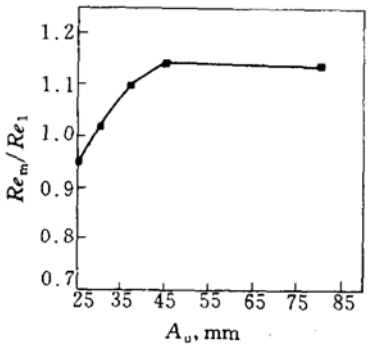

Figure 11 Predicted results on ratio of Re_m to Re_1 vs. A_u for $s=5$ ($W_1=10\text{m}\cdot\text{s}^{-1}$)

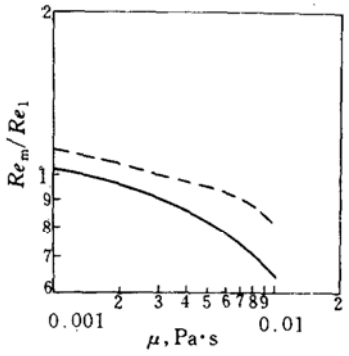

Figure 12 Predicted results on ratio of Re_m to Re_1 vs. viscosity ($W_1=10\text{m}\cdot\text{s}^{-1}$)
----- $s=5$; —— $s=10$

5 CONCLUSIONS

A numerical program is developed for the hydrodynamic simulation of homogeneous jet loop reactors. The results agree well with experimental data reported in the literature. The reasonable results are obtained when this is used to analyze the influence of configurational parameters and liquid viscosity on the flow. All the above results suggest that this numerical simulation is a powerful tool in the research and development of loop reactors.

NOMENCLATURE

A_0	spacing atop draft tube, m
A_u	spacing below draft tube, m
D	internal diameter of loop reactor, m
D_1	diameter of liquid jet nozzle, m
D_E	mean diameter of draft tube, m
H	filling height of reactor, m
k	turbulent kinetic energy
L_e	length of draft tube, m
L_ε	eddy length scale of turbulence, m
$\dot{M}_1$	jet flow rate, $\text{kg}\cdot\text{s}^{-1}$
$\dot{M}_2$	circulation flow rate, $\text{kg}\cdot\text{s}^{-1}$
$\dot{M}_3$	total mass flow, $\text{kg}\cdot\text{s}^{-1}$
n_u	circulation number
p	pressure, Pa
Re_m	Reynolds number of circulation
Re_1	Reynolds number of liquid jet
s	ratio of height to diameter
U	velocity, $\text{m}\cdot\text{s}^{-1}$
W_1	jet liquid velocity, $\text{m}\cdot\text{s}^{-1}$
W_m	mean circulation velocity, $\text{m}\cdot\text{s}^{-1}$
x	coordinate
γ	kinematic viscosity, $\text{m}^2\cdot\text{s}^{-1}$
ε	turbulent energy dissipation
μ	viscosity, Pa·s
ρ	density, $\text{kg}\cdot\text{m}^{-3}$

Subscripts

E	east
e	effective
N	north
S	south
t	turbulent
W	west
1	radial direction
2	axial direction

REFERENCES

1 Blenke, H., *Adv. Biochem. Eng.*, **13**, 121 (1979) .
2 Blenke, H., Biotechnology, **2**, 463, eds. Rehm, H.-J., VCH, Weinheim (1985) .
3 Cheng Linna, Zhu Weixing and Ouyang Fan, *Chemical Reaction Engineering and Technology (China)* , **8**, 185 (1992) .
4 Julius, W. H. and Michael M., World Congress III of Chemical Engineering, Science and Technology Press, Beijing, China, **3**, 358 (1986) .
5 Zenz, F. A., *Chem. Eng. Prog.*, **89** (8) , 51 (1993) .
6 Lin Wencai, *Loop Reactors: Theoretical and Experimental Studies on Hydrodynamic Characteristics*, Ph. D dissertation, Institute of Chemical Metallurgy, Academia Sinica, Beijing (1993) .
7 Sun Keshen, *Chem. Eng. (China)* , (5) , 41 (1980) .
8 White M. F., Viscous Fluid Flow, McGraw-Hill, Inc., New York (1974) .
9 Jones, W. P. and Launder, B. E., *Int. J. Heat Mass Transfer*, **16**, 1119 (1973) .
10 Patankar, S. V., Numerical Heat Transfer and Fluid Flow, Hemisphere, Washington, D. C. (1980) .
11 Settari, A. and Aziz, K., *SIAM J. Numer. Anal.*, **10**, 506 (1973) .
12 Shekhar, R. and Evans, J. W., *Metallurgical Transactions*, **21B**, 191 (1990) .